Space Weather

RESEARCH ARTICLE
10.1029/2025SW004854

PPP-RTK Atmospheric Correction Generation and Service Applicability: A Case Study During Typhoon Saola and Moderate Geomagnetic Disturbances in Hong Kong

Jiahuan Hu[1], Xuanyu Qu[1,2,3,4], Pan Li[5], Mengyu Ding[1], Jiadi Dai[5], Xiaoli Ding[1,2,3,4], and Wu Chen[1,2,3]

[1]Department of Land Surveying and Geo-Informatics, The Hong Kong Polytechnic University, Hong Kong, China, [2]Research Institute for Land and Space, The Hong Kong Polytechnic University, Hong Kong, China, [3]Shenzhen Research Institute, The Hong Kong Polytechnic University, Shenzhen, China, [4]Guangdong–Hong Kong Joint Research Laboratory for Marine Infrastructure, Hong Kong, China, [5]College of Geology Engineering and Geomatics, Chang'an University, Xi'an, China

Abstract Complex space weather, such as typhoons and solar activity, can cause heavy rainfall and ionospheric disturbances, affecting the quality of Global Navigation Satellite System (GNSS) signals. Among GNSS positioning techniques, Precise Point Positioning Real-time Kinematic (PPP-RTK) uses atmospheric corrections and bias products to achieve fast convergence and high accuracy solutions, with the quality of ionospheric and tropospheric corrections being critical to PPP-RTK performance. While most research focuses on improving user positioning accuracy, few studies address PPP-RTK applicability under complex space weather. This study uses GNSS data from Hong Kong to generate and verify PPP-RTK corrections during Typhoon Saola and a moderate geomagnetic disturbance in solar cycle 25. Results show that derived tropospheric zenith wet delay (ZWD) aligns with historical rainfall data, and ZWD model residuals are positively correlated with the typhoon process, with standard deviations below 4 mm. The ionospheric interpolation errors increase before and after landfall, and the possible reason is that the ionospheric perturbations in the eye of the storm are fewer than those at the edges of the typhoon. Across days, ionospheric interpolation error standard deviations range from 5 to 10 cm. PPP-RTK validation using these corrections achieves 1–2 cm accuracy with near-instantaneous convergence in east and north directions, while 2–5 min are needed for the up direction to converge to 2–6 cm accuracy. The assessment and validation confirm the high precision of atmospheric corrections and the applicability of PPP-RTK during typhoon Saola and moderate geomagnetic disturbances in a dense network in Hong Kong.

Plain Language Summary Satellite navigation systems like GPS help us find our way when driving, flying drones, or doing land surveys. But bad weather, such as typhoons and solar activity can disturb the atmosphere and make these systems less accurate. In this study, we looked at how Typhoon Saola and medium solar activity affect the accuracy of a high-precision positioning method called PPP-RTK in Hong Kong, a place often hit by typhoons. We found that, even during heavy rain and storms, our corrections for weather and atmospheric changes worked well and matched real rainfall data. Atmospheric corrections quality is slightly affected during typhoons. When we tested the positioning system, it still gave very accurate results (within a few centimeters), even during typhoons and periods of increased solar activity. This means that, with the right corrections, PPP-RTK can stay reliable even in tough weather. Our results are important for anyone who needs precise location information, like drivers, drone pilots, and emergency services. They show that satellite navigation can still be trusted during storms, as long as we use good correction methods.

Key Points:

- Precise Point Positioning Real-time Kinematic stays accurate during typhoon Saola and moderate solar activity with well-modeled atmospheric corrections
- Atmospheric effects caused by severe weather can be effectively corrected, ensuring centimeter-level Global Navigation Satellite System (GNSS) positioning accuracy in Hong Kong
- These results support the reliable operation of GNSS-based applications, including UAVs, even during moderate typhoons and solar activity

Correspondence to:
X. Qu,
xuany.qu@connect.polyu.hk

Citation:
Hu, J., Qu, X., Li, P., Ding, M., Dai, J., Ding, X., & Chen, W. (2026). PPP-RTK Atmospheric correction generation and service applicability: A case study during Typhoon Saola and moderate geomagnetic disturbances in Hong Kong. *Space Weather*, *24*, e2025SW004854. https://doi.org/10.1029/2025SW004854

Received 25 NOV 2025
Accepted 1 MAR 2026

Author Contributions:
Conceptualization: Jiahuan Hu, Xuanyu Qu, Pan Li, Wu Chen
Data curation: Jiahuan Hu, Xuanyu Qu, Mengyu Ding
Formal analysis: Jiahuan Hu, Xuanyu Qu, Pan Li, Mengyu Ding, Jiadi Dai
Funding acquisition: Xuanyu Qu
Software: Jiahuan Hu, Pan Li, Jiadi Dai
Supervision: Xiaoli Ding, Wu Chen
Writing – original draft: Jiahuan Hu, Xuanyu Qu
Writing – review & editing: Jiahuan Hu, Xuanyu Qu, Pan Li, Mengyu Ding, Jiadi Dai, Xiaoli Ding, Wu Chen

1. Introduction

With the capability of providing accurate spatial information for users worldwide, Global Navigation Satellite System (GNSS) has garnered significant attention in recent years. Precise Point Positioning Real-time Kinematic (PPP-RTK) technology, which utilizes atmospheric corrections and bias products as constraints in user algorithms, has the potential to achieve instantaneous high-accuracy positioning performance (Huang et al., 2023; Teunissen et al., 2010; Wübbena et al., 2005). Theoretically, accurately modeled atmospheric corrections could facilitate fast-convergence and high-precision solutions, that is, the more accurate the atmospheric corrections, the better the positioning performance (Hu et al., 2023). However, there are complex space weathers such as

severe convective weather and solar activities that could affect the propagation of electromagnetic wave signals, which would thereby influence the atmospheric correction generation and potentially affect the positioning performance (Xue et al., 2025).

The tropospheric and ionospheric refractions are two major error sources that affect the GNSS signals (Qu et al., 2025). The troposphere is the primary site of meteorological phenomena, including the formation and evolution of tropical cyclones such as typhoons, while the ionosphere is easily affected by solar activities which can significantly alter ionospheric density and composition. In Standard Point Positioning, the ionospheric and tropospheric refractions can be corrected using empirical models (Klobuchar, 1987), while in high-precision positioning, the atmospheric effects are either directly estimated (e.g., uncombined PPP and PPP-RTK) or eliminated (e.g., ionospheric-free PPP and double-differenced RTK) (Kouba & Héroux, 2001). The effect of complex space weather on GNSS precise positioning performance has been widely assessed, which primarily concentrates on RTK and PPP (Carter et al., 2023; Danilchuk et al., 2025). Paziewski et al. (2022) found that ambiguity resolution in RTK was significantly affected during ionospheric storms, while less effects are observed in single-frequency PPP. He et al. (2023) noticed that the Percentage of Affected Satellites index showed significant anomaly changes during the moderate geomagnetic storm. To mitigate the negative effects of complex space weather, refined cycle slip detection methods are proposed, results showed that the PPP performance can be largely improved during ionospheric irregularities (Li et al., 2025; Luo, Du, Lou et al., 2022). Moreover, rate of total electron content index (ROTI)-based stochastic model also demonstrated PPP accuracy enhancement of approximately 13% compared to the elevation-dependent weighting function (Luo, Du, Galera et al., 2022). Most of the above-mentioned progress is about the ionospheric events, and few of them address the effect of the troposphere on positioning performance.

Generally, PPP-RTK positioning performance is expected to reach decimeter- or centimeter-level with geodetic-grade receivers (Li, Cui et al., 2022; Odijk et al., 2016). Regional ionospheric and tropospheric models are built on the server and broadcast to users. As the regional atmospheric corrections are typically at high precision levels, users can apply proper constraints to the atmospheric corrections and obtain satisfactory positioning results (Zhang et al., 2022). Ma et al. (2020) conducted PPP-RTK with different combinations of constellations, and reached positioning accuracy of ∼2 cm with GPS, GLONASS, Galileo, and BDS. It is also concluded by Li, Wang et al. (2022) that incorporating multi-frequency measurements in PPP-RTK could further improve the positioning accuracy and ambiguity fix rate. Recently, Zhang et al. (2025) utilized the multi-GNSS and multi-frequency PPP-RTK model to obtain instantaneous convergence with high-confidence atmospheric products, maintaining positioning accuracy within 2.5 cm. Despite much progress in PPP-RTK reported in existing research, most of them focused on the general PPP-RTK performance, that is, no specific attention has been paid to PPP-RTK atmosphere correction generation and applicability during complex space weather.

It is widely recognized that there would be severe convective weather during typhoon events, however, ionospheric disturbances can also be caused by typhoon event (Li, Zhang, et al., 2024, Li, Liu et al., 2024). Even with a distance of ∼1,050 km from the typhoon eye, ionospheric disturbances could be observed (Chen et al., 2020). Xu et al. (2020) found that, before Typhoon Meranti, Sarika, and Haima made landfall, the probability and intensity of ionospheric scintillation of GPS satellites in the affected areas increased. Yu et al. (2022) reported significant ionospheric disturbances during the passage of super typhoon Hato in 2017, in which the TEC above Hong Kong increased from 33.5 TEC unit (TECU) to 62.0 TECU on the landfall day. Moreover, Nie et al. (2024) found the presence of equatorial plasma bubbles that caused prominent amplitude scintillation and TEC fluctuations during typhoon Saola, which led to PPP performance degradation from decimeter-to meter-level.

Not only the typhoon event, but also the solar activities could cause ionospheric disturbances, which will further bring risks in obtaining reliable GNSS positioning results. Positioning accuracy degradation has been noticed during complex space weather (Moreno et al., 2011). Rodríguez-Bilbao et al. (2015) further confirmed that high TEC variations lead to increased positioning errors. Luo et al. (2018) performed GPS PPP experiments under different geomagnetic storm conditions, positioning accuracy of 0.4 m, 0.7 m, and 1.1 m was obtained during moderate, intense, and super storms, while the positioning error was only 0.2 m under quiet conditions. Later, Demyanov and Yasyukevich (2021) reported that kinematic PPP solutions can deteriorate to a few meters with radio bursts caused by extreme space weather. The results from Li, Zhang, et al. (2024), Li, Liu et al. (2024) further demonstrated that static PPP convergence time is increased by more than 30 min during geomagnetic storms compared to magnetic quiet days.

With the extensive application of PPP-RTK technology, it is also questionable whether PPP-RTK is applicable in complex space weather such as typhoon and medium solar activity, as reliable and accurate positioning solutions are required by safety-related applications such as autonomous driving and drone navigation. As two major corrections in PPP-RTK, the ionospheric and tropospheric correction quality play a vital importance in obtaining satisfying positioning results. Therefore, it is necessary to carry out this research to closely and comprehensively investigate the quality of PPP-RTK atmospheric corrections and verify the applicability of PPP-RTK during severe convective weather and medium solar activity. The contribution and novelty of this study is as follows:

1. Considering that most current research concentrates solely on user performance during ionospheric disturbances, the PPP-RTK ionospheric and tropospheric corrections generated at server are comprehensively evaluated during typhoon Saola and medium solar activity for the first time. Key indices including atmospheric model correction time series, model residuals, and model interpolation errors are comprehensively assessed.
2. While existing research on PPP-RTK mainly reported results under normal conditions, this study detailed presents and compares the correction quality and positioning performance for different periods of typhoon Saola, for example, before and during landfall, and extinction.
3. Despite research focused on reporting observed ionospheric disturbances during typhoons has been conducted, this study, for the first time, quantitatively assesses how the typhoon process affects the PPP-RTK ionospheric and tropospheric corrections, which takes one step closer to the positioning performance effect by typhoon.

In the rest of the article, the GNSS observation functions, as well as the atmospheric modeling methods, are introduced briefly, followed by descriptions of the data used and a typhoon event. The detailed assessment and comparison of ionospheric and tropospheric corrections in PPP-RTK is conducted. Finally, positioning verification is carried out.

2. Methodology

Taking advantage of the un-differenced and un-combined PPP model, the ionospheric and tropospheric refractions can be simultaneously estimated along with the coordinate parameters. For GNSS phase and code measurements collected by a receiver, the raw observation equation can be expressed as

$$\begin{cases} P_j^s = \rho^s + c(dt_r + isb^{sys} - dt^s) + \gamma_j I_1^s + T^s + b_j^s + b_{r,j} + \varepsilon_j^s \\ L_j^s = \rho^s + c(dt_r + isb^{sys} - dt^s) - \gamma_j I_1^s + T^s + \lambda_j \tilde{N}_j^s + \xi_j^s \end{cases} \tag{1}$$

with

$$T^s = mf_h^s \cdot \mathrm{ZHD} + mf_w^s \cdot \mathrm{ZWD} \tag{2}$$

$$\tilde{N}_j^s = N_j^s + B_j^s + B_{r,j} \tag{3}$$

where s and j represent satellite and frequency, respectively. P and L are pseudorange and carrier phase measurements in units of meters, respectively. ρ is the satellite-receiver geometrical distance, and c is the speed of light. dt_r is receiver clock offset at time of arrival, and dt^s is satellite clock offset at time of transmission. isb^{sys} is the inter-system bias (ISB) with respect to GPS, that is, when the constellation is not GPS, a system-related ISB should be estimated. γ_j is the ionospheric frequency coefficient on the jth frequency, and $\gamma_j = \left(f_1/f_j\right)^2$, where f denotes the frequency. I_1^s is the slant ionospheric effect on the first frequency. T^s refers to the slant tropospheric delay which comprises the hydrostatic and wet components, and can be calculated using the mapping functions mf and the zenith hydrostatic delay and zenith wet delay (ZWD). λ_j is the wavelength, and $\tilde{N}_j^s$ is the float ambiguity. $\tilde{N}_j^s$ consists of integer ambiguity N_j^s, satellite phase hardware bias B_j^s and receiver phase hardware bias $B_{r,j}$. b_j^s and $b_{r,j}$ are code hardware biases for the satellite and receiver, respectively. ε_j^s and ξ_j^s are code and phase observation noise coupled with multipath and unmodeled errors.

With applying proper model corrections including relativistic effects, tide loading, satellite and receiver antenna corrections, phase wind-up, differential code bias, the PPP float solution can be obtained (Kouba, 2009; Wu et al., 1993). To improve the accuracy of estimated parameters, carrier phase ambiguity resolution is conducted. Since this study mainly focuses on atmospheric corrections, and PPP AR methods have been widely discussed in existing literature (Geng et al., 2022; Hu et al., 2020), no detailed PPP user algorithm is introduced in this study. With successfully estimated atmospheric parameters from each regional station, the tropospheric ZWD can be modeled using the Modified Optimal Fitting Coefficients (MOFC) model (Cui et al., 2022), as

$$\mathrm{ZWD}(dL, dB, dH) = \left(\sum_{i=0}^{2} \sum_{j=0}^{2} a_{ij} \cdot (dL)^i \cdot (dB)^j \right) e^{dH/a_k} \tag{4}$$

with

$$\begin{cases} dL = L_i - \overline{L} \\ dB = B_i - \overline{B} \\ dH = -(H_i - H_{\min})/(H_{\max} - H_{\min}) \end{cases} \tag{5}$$

where a_{ij} and a_k are the fitted coefficients of the MOFC model. dL, dB, and dH are the longitude, latitude, and height differences between the model center $(\overline{L}, \overline{B})$ and the user position (L_i, B_i), $H_{\min}$ and $H_{\max}$ are the minimum and maximum height used in fitting the model. With at least 7 stations used to fit the coefficients in Equation 4, ZWD model value can be built with a given position in the modeled regional area.

Different from the ZWD for which obvious differences might be observed in different areas of medium and small regions, the ionospheric refractions for signals from the same satellite exhibit smaller differences because of similar propagation paths when the region is small, for example, within 50 km. There are mainly three methods of applying ionospheric corrections, that is, (a) modeling the slant total electron content (STEC) corrections using different functions and broadcasting the coefficients (Huang et al., 2025; Li et al., 2022), (b) modeling the regional vertical total electron content (VTEC) together with differential code bias corrections (Chen et al., 2023), and (c) directly interpolate the ionospheric corrections from nearby server stations (Hu et al., 2025). In regional PPP-RTK network, the slant corrections are usually used, as the modeling of VTEC corrections might be affected by the unperfect models and ionospheric mapping functions. Moreover, given the test region is relatively small (e.g., inter-station distance is less than 50 km in this study), and the expected performance would be similar when directly using interpolated corrections and STEC coefficients, in this study, the ionospheric corrections for users are calculated using ionospheric corrections from three nearby server sites, and inverse distance weight (IDW) interpolation is utilized, as

$$\mathrm{STEC}_{\mathrm{user}} = \left(\sum_{i=1}^{3} \frac{\mathrm{STEC}_i}{\|x - x_i\|} \right) \Big/ \left(\sum_{i=1}^{3} \frac{1}{\|x - x_i\|} \right) \tag{6}$$

where STEC represents the STEC, x is the user coordinates, and x_i is the position for the ith server station. The criteria for selecting the server stations is that, the user station should be close to the center of the triangulation network formed by three server stations. With the atmospheric model formulated as Equations 4–6, the detailed assessment of the atmospheric correction applicability during severe convective weather and medium solar activity can be conducted.

3. Experiment

GNSS data from Hong Kong was selected to conduct the experiment validation, as the attitude of this region is low and it is easily affected by tropical cyclones, indicating that the ionosphere activities and the convective weather frequently occur. Therefore, 17 CORS stations in Hong Kong were selected in generating the atmospheric corrections, and the distribution is shown as Figure 1. Except for the station KYC1 which tracked only GPS signals, other stations were able to receive GNSS signals from GPS, Galileo,

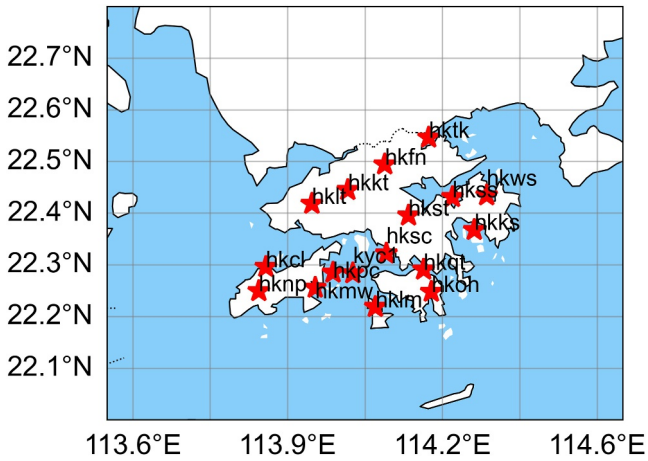

Figure 1. Distribution of 17 Hong Kong CORS stations used in this study.

GLONASS, and BDS. The minimum inter-station distance is 4.8 km (HKMW-HKPC), while the maximum distance is 46.6 km (HKCL-HKWS). The average inter-station distance between rover and server stations is 11.2 km, which is a dense regional network. GNSS Data from the 23rd August to the 10 September 2023 was processed, as this period covers a typhoon event (Saola) from the 23rd August to 4th September, a medium ionospheric activity during 2nd–3rd September, and severe convective weather during 7th–8th September.

Typhoon Saola formed over the northwestern Pacific Ocean on the 23 August 2023, about 670 km southeast of Kaohsiung. It then moved westward toward the South China coast. Comparing the peak intensity with historical typhoons, Typhoon Saola (year 2023) was stronger than Hato (year 2017) but weaker than the exceptionally powerful Meranti (year 2016). The Hong Kong Observatory (HKO) issued the No. 1 Hurricane Signal on the 30th August and the No. 8 Signal on the 1st September, when the typhoon was about 630 and 280 km from Hong Kong, respectively. As Saola approached further, the HKO raised the warning to Signal No. 10 (the highest level) when the storm was around 50 km from the city. During the typhoon, the HKO recorded wind speeds of up to 52.5 m/s and total rainfall exceeding 250 mm. On the 7th and 8th September, Hong Kong experienced extreme rainfall shortly after the typhoon. The HKO reported over 100 mm of precipitation across most parts of the region within a 24-hr period, with localized areas receiving more than 400 mm, marking one of the heaviest rain events in recent decades.

4. Results

Detailed quality assessment of the tropospheric and ionospheric corrections is conducted in this section, followed by PPP-RTK positioning validation to demonstrate the effectiveness and applicability of the generated atmospheric corrections during the selected periods.

4.1. Tropospheric Correction

The evaluation of tropospheric corrections contains the analysis of daily derived ZWD time series, the ZWD model residuals, as well as the generated ZWD model map within Hong Kong. Firstly, the time series of estimated ZWDs for each station for 19 days are illustrated in Figure 2, in which the historical rainfall records from HKO are also presented in the bottom panel. It should be noted that the daily records from the HKO used local time (UTC +8), therefore, when assessing the tropospheric corrections, the results of the days before and after the rainfall presented in Figure 1 might also be affected. ZWD is positively correlated with precipitable water vapor, therefore, it is significant that when the historical rainfall records were at high levels on the 7th and 8th September, the estimated ZWD for all stations also reached the peak. For normal conditions with limited or without rainfall (e.g., 23rd–30th August), the ZWDs are at the same levels. The differences of ZWD among different stations are mostly below 5 cm on normal days, indicating a relatively similar weather condition within Hong Kong.

With estimated ZWDs from all stations, a ZWD model can be fitted, and the ZWD model residuals for each station can be calculated by differencing the model-calculated value and the PPP-derived values. The box plot of the absolute ZWD residuals is depicted in Figure 3, the historical rainfall records and the distance from Typhoon center to Hong Kong are also illustrated for an intuitive comparison. The medium values of absolute ZWD residuals for different days are all around 2 mm, indicating the built model is of high precision despite there is severe convective weather. For the 2 days with heavy rainfall, the upper whiskers of the box plot are higher (at ∼8 mm). The outliers are significant for several days, which could probably be caused by the differences in ZWDs among different stations during complex weather, for example, part of Hong Kong was rainy while the rest were not.

Statistical analysis is also conducted to quantitatively assess the tropospheric model. Key indices including residual standard deviation, the 68th, 90th, and 95th percentiles (PCT) of the absolute ZWD model residuals, as well

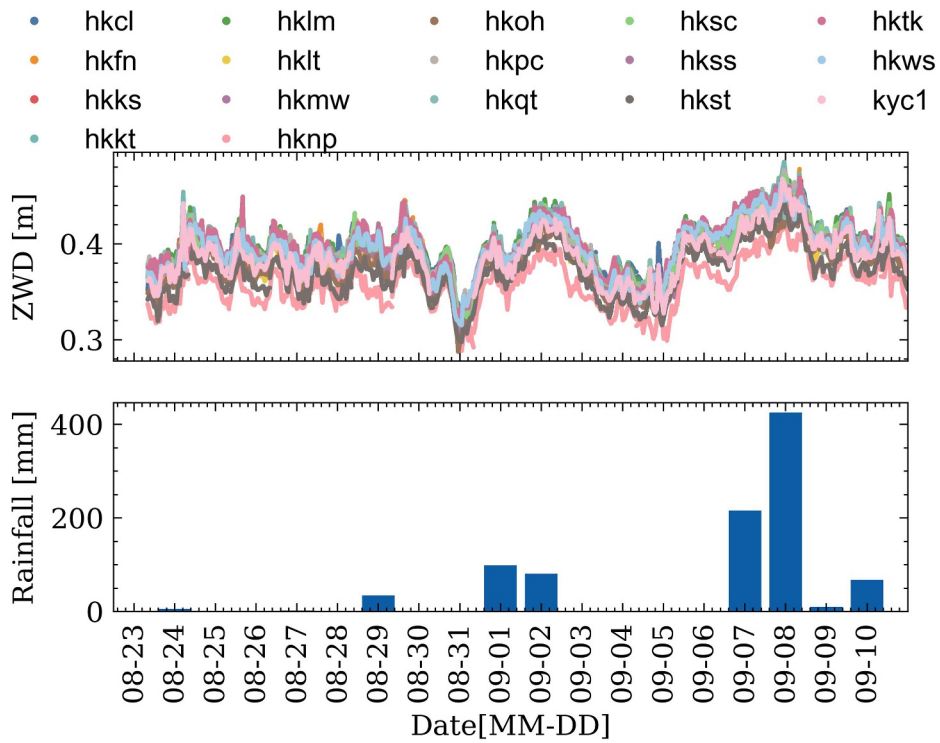

Figure 2. Time series of estimated zenith wet delay and corresponding reference rainfall data (Hong Kong local time).

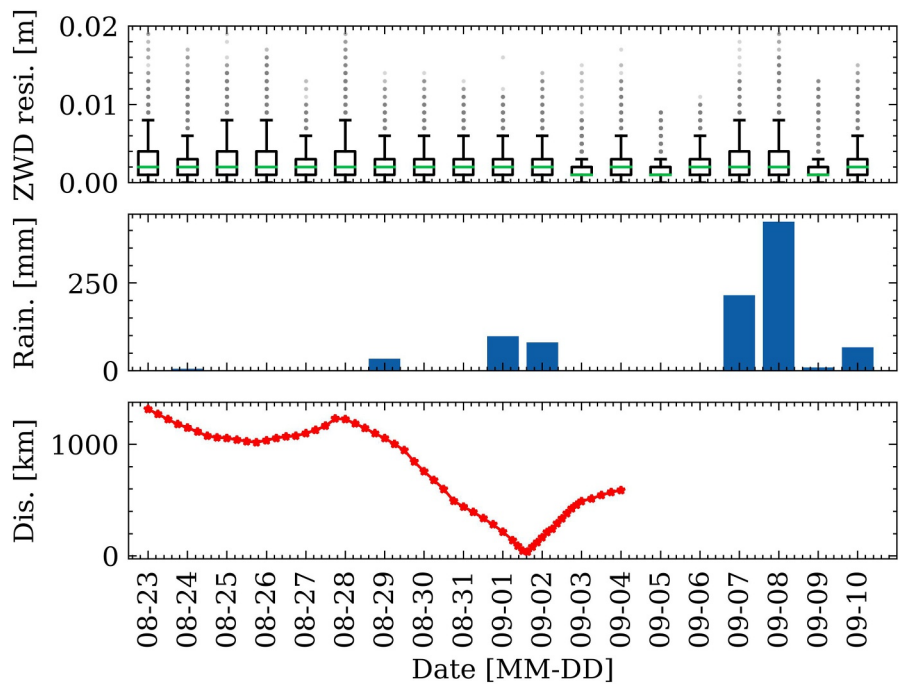

Figure 3. Box plot of absolute zenith wet delay model residuals along with historical rainfall data and the distance of the Typhoon center to Hong Kong.

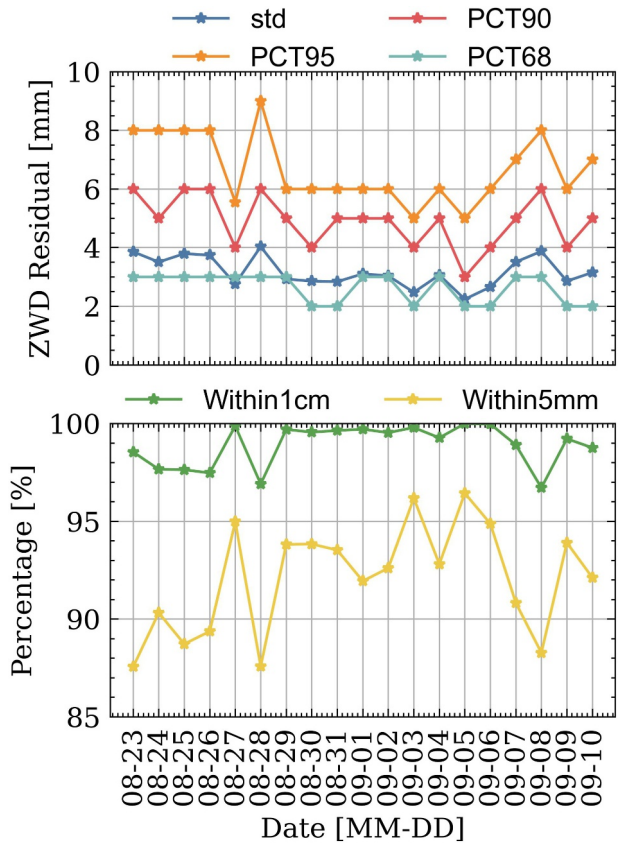

Figure 4. Average statistics of zenith wet delay model residuals for all stations on different days, with std calculated using raw values, and PCTs calculated with absolute residual values.

as the percentages of residuals within 1 cm and 5 mm are calculated and shown in Figure 4. Noting that the STDs are calculated using raw values, that is, without the absolute operator, while other statistics are calculated with the absolute residuals. The STD and PCT68 values are relatively stable across different days, while the variations for other indices are more significant. It is interesting to note that the ZWD model residuals increase with the coming of large rainfall from the 5th to 8th September, with PCT90 increasing from 3 to 6 mm, and PCT95 increasing from 5 to 8 mm. Despite the severe convective weather, the percentage of ZWD model residuals within 5 mm still exceeds 88%, inferring that the PPP-RTK tropospheric models generated in this study are highly applicable during complex conditions.

Considering that significant ZWD model residual outliers are noticed in Figure 3, an in-depth analysis regarding the distribution of daily ZWD model residuals is necessary to guarantee that the expected generalized normal distribution is obtained, and the results are shown in Figure 5. The mean values are all close to zero, while the STDs range from 0.22 to 0.40 cm, indicating that the ZWD model is accurately fitted, and the outliers are not because of the model itself. For all dates, most of the residuals are within 1 cm. For days with significant residual outliers, the STDs are almost larger than 0.35 cm, while those with fewer outliers have smaller STDs (e.g., below 0.3 cm). Again, the possible reason is the different weather conditions near different stations.

To have an intuitive view of the built ZWD model, the model maps in the Hong Kong region at local time 8 a.m. for 16 days are plotted and illustrated in Figure 6. On the 1st, 2nd, and 7th–10th September, the ZWD model values are large, which is consistent with the historical rainfall records shown in Figure 3. Moreover, it is worth noting that on the 28th August and 8th September, the ZWD map indicates varying weather conditions in Hong Kong, with clear differences in ZWD values. Because of the differences, the ZWD model residuals are larger these days, which further confirms our previous conclusion that the larger residuals and significant outliers in ZWD model residuals are probably caused by the different weather conditions within Hong Kong. Based on the analysis of the ZWD model, the generated tropospheric corrections in this study are at high-precision levels, and have great potential in enhancing PPP-RTK user performance in selected periods in this study.

4.2. Ionospheric Correction

Different from the ZWD models which are highly related to the convective weather, the ionospheric models are affected by the ionospheric activities and typhoon events. Therefore, to evaluate the performance of ionospheric corrections during the Typhoon event, key indices including the date-specific and station-specific interpolation residuals, as well as the ionospheric interpolation precision map are comprehensively assessed.

The STEC corrections for a given position can be calculated using STEC estimates from three nearby stations, taking daily PPP-AR-derived STECs as references, the interpolation residuals are represented as the differences between interpolated values and estimated values. Figure 7 illustrates the box plot of the absolute values of interpolation errors for different days. The medium interpolation errors (green lines in the boxes) are all below 0.05 m across different days, and the upper whiskers (75th percentile) are ∼0.1 m, indicating the interpolated STEC corrections are of high precision. While the majority of the interpolation errors are small, some outliers can still be noticed, which could even reach half a meter and mostly come from low-elevation satellites.

Disturbance storm time index (Dst), interplanetary magnetic field of z-component (IMF-Bz), planetary K index (Kp), and ROTI are the four commonly used indices in indicating the ionospheric activities. To clearly show

10.1029/2025SW004854

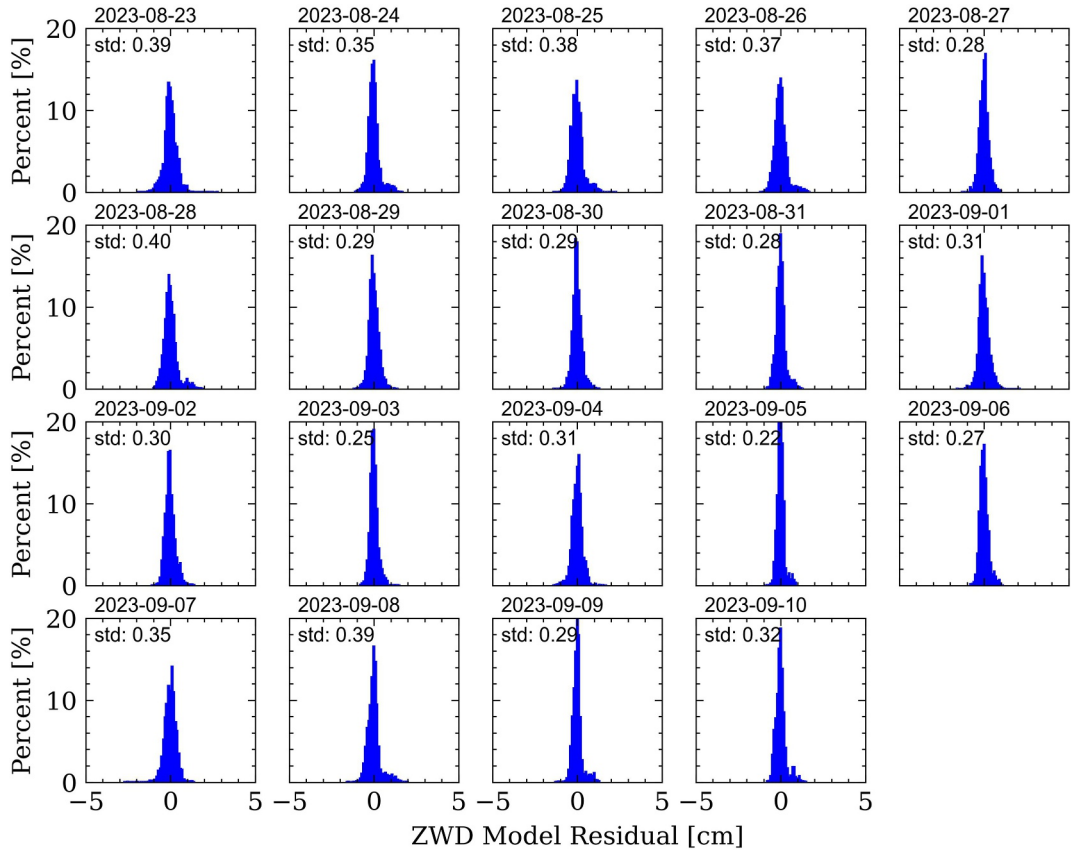

Figure 5. Zenith wet delay model residual distributions for all stations on different days.

whether there is significant solar activity which could affect the ionosphere modeling, the time series of Dst, IMF-Bz, and Kp are plotted in Figure 8, and the ROTI time series of all BDS satellites for station HKCL are shown in Figure 9. From Figure 8, most of the Kp indices of geomagnetic activity are below 4, while during the 2nd–3rd September, the Kp values are larger than 4, indicating the occurrence of medium ionospheric disturbances. Similarly, a significant decreasing trend of the Dst is found within the same period. For these 2 days, despite moderate geomagnetic disturbances occur, the interpolated STECs are at high precision level, indicating that the derived STEC corrections in the PPP-RTK algorithm are less affected by such medium ionospheric activities. In terms of the ROTI time series in Figure 9, with different colors representing different BDS satellites, ionospheric scintillation can be noticed except for periods between 1st September and 5th September, which therefore infer that the generated ionospheric corrections are also applicable when ionospheric scintillations are observed.

Figure 10 further concludes the statistics of the interpolated STEC residuals for different days. Almost all indices follow similar trends. For most days, the 90th percentile of interpolation errors are below 0.1 m. Two significant increasing trends in interpolation errors are found: 28th–31st August and 1st–7th September, which are highly consistent with the distance between the Typhoon center to Hong Kong by comparing Figure 10 with the distance shown in Figure 3. Moreover, small interpolation errors on the 1st September are obtained, which is exactly the time when the Typhoon eye is near to Hong Kong. It was confirmed by existing research that the ionospheric perturbations in the eye of the storm are fewer than those at the edges of the typhoon (Chen et al., 2020; Freeshah et al., 2021; Li et al., 2017), which is consistent with the statistical results of the STEC interpolation errors in Figure 9. Furthermore, the errors increase from the 1st–7th September and then start to be reduced, which could be explained by the ionospheric disturbances caused along with the extinction process of Typhoon, as reported by Du et al. (2023).

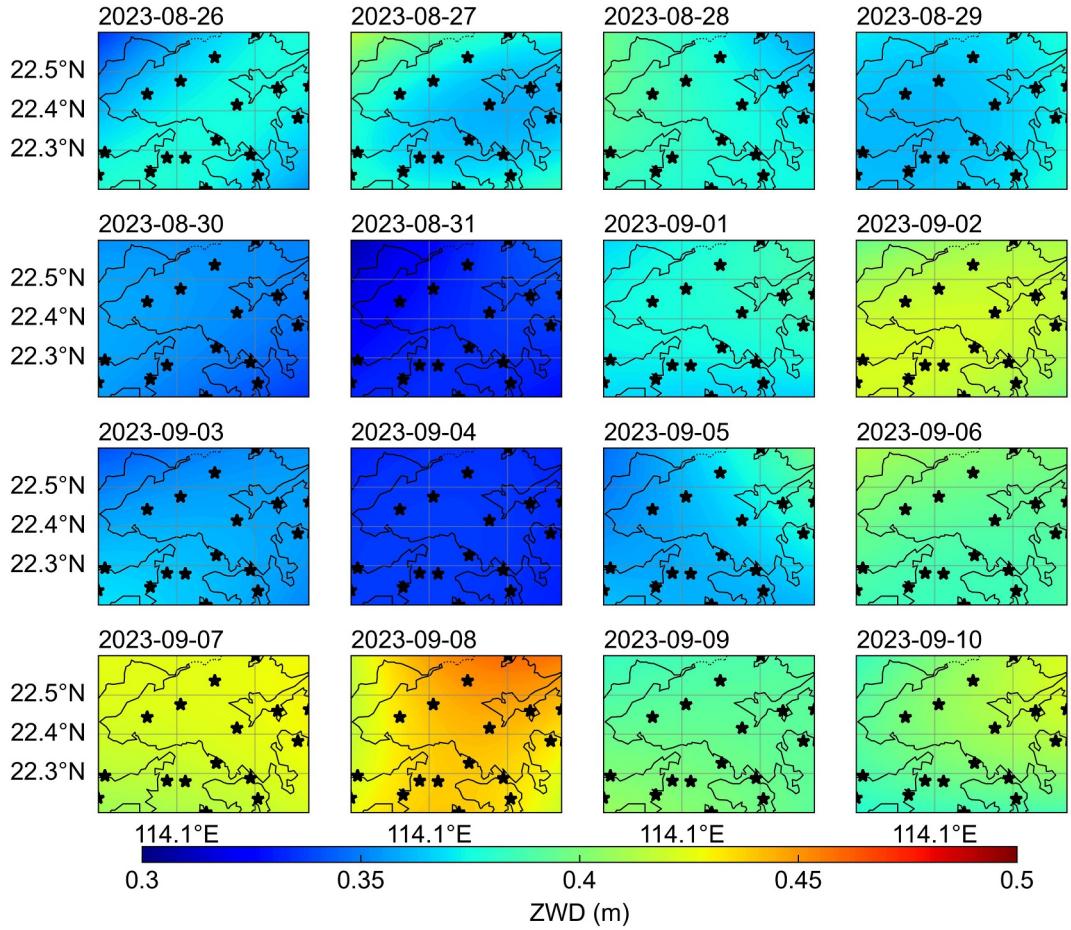

Figure 6. Zenith wet delay model in Hong Kong region for 16 days (Local time 08:00).

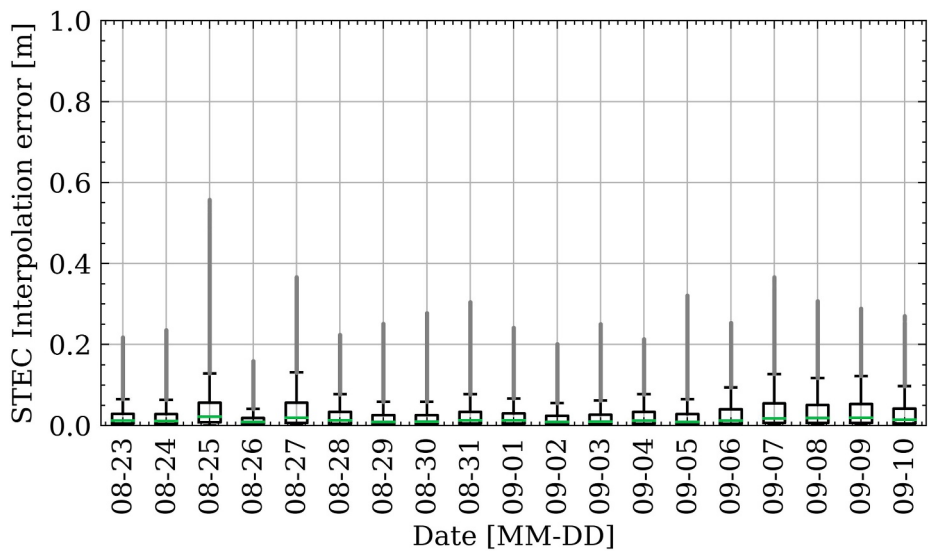

Figure 7. Box plot of absolute slant total electron content interpolation errors for different days.

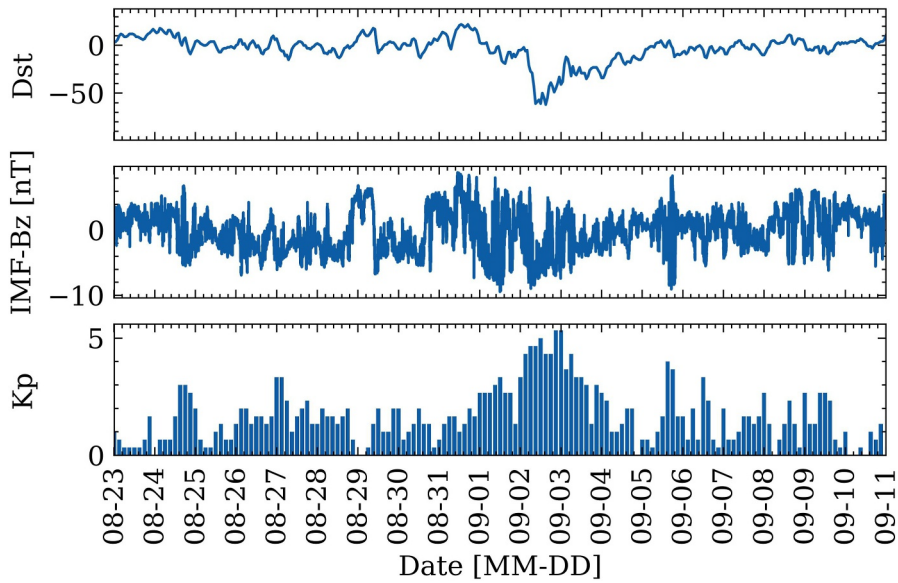

Figure 8. Dst, IMF-Bz and Kp indices during the Typhoon event.

To have an in-depth insight into station-specific interpolation errors, Figure 11 illustrates the STDs of interpolation errors for each station on different days, in which the dots represent the stations, and the color represents the magnitude of the STD. In the main service areas, most of the STDs are within 0.05 m. In contrast, the STDs are relatively larger for the stations at the edge of the CORS network, for example, the lower left station HKNP and the upper right station HKTK, whose STDs can even reach 0.2 m during ionospheric disturbances. Similar interpolation accuracy degradation near network boundaries was reported

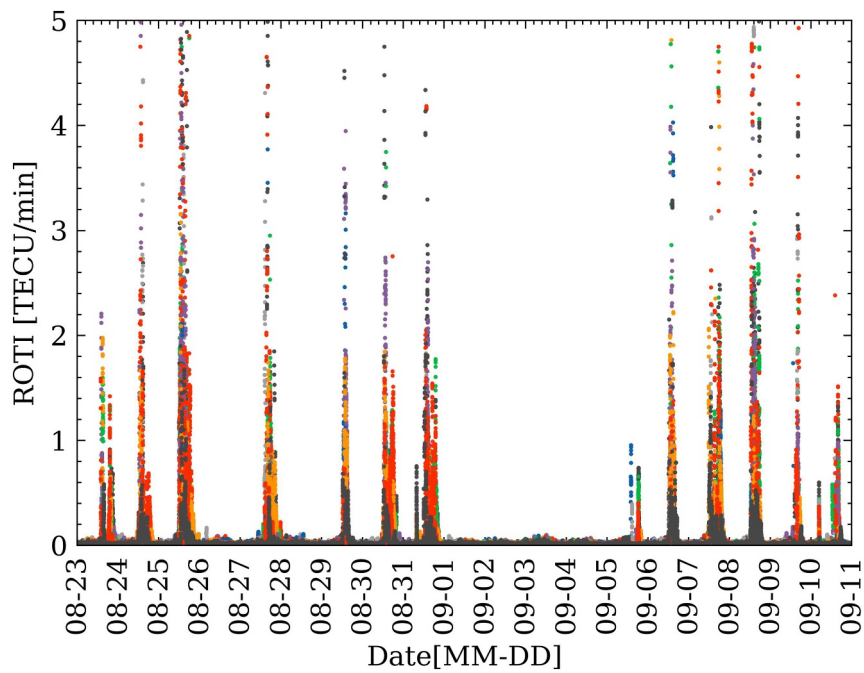

Figure 9. Rate of TEC index time series of all BDS satellites for station HKCL.

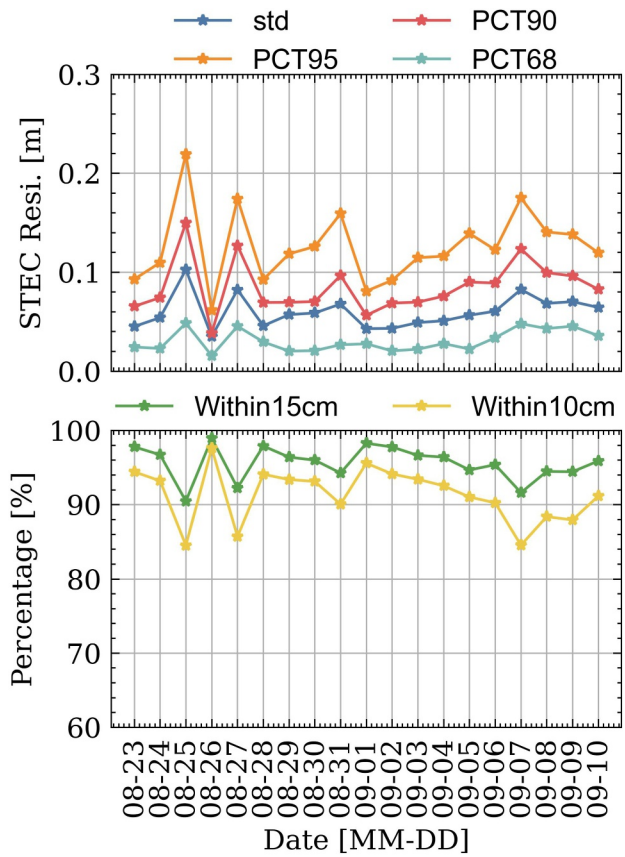

Figure 10. Average statistics of slant total electron content interpolation residuals for all stations on different days, with std calculated using raw values, and PCTs calculated with absolute residual values.

by Hu et al. (2023). There are possibly two reasons for the poor interpolation performance at peripheral stations: (a) the average distances between reference and user stations used for interpolating ionospheric corrections at stations HKNP and HKTK are 20.2 and 15.9 km, which are relatively longer compared to the central stations, and (b) the geometry distribution of the used reference stations for peripheral stations is poorer compared to the central stations, which is similar to the relationship between expected positioning performance and satellite geometry, that is, a larger position dilution of precision usually indicate a poor satellite geometry and degraded positioning solutions. Since this study adopts the IDW for interpolation, an alternative interpolation method (e.g., kriging) might help mitigate the interpolation boundary effects.

4.3. Positioning Validation With Hong Kong CORS Stations

A PPP-RTK kinematic positioning experiment is carried out to validate the applicability of generated atmospheric corrections during complex space weather. The atmospheric corrections are applied as external constraints in the PPP-RTK user algorithm, positioning errors and convergence time for the east, north, and up directions are calculated and illustrated in Figure 12. The positioning accuracy is the root mean square errors after convergence, and the convergence time is defined as the time taken to reach positioning errors below 1 dm and last for at least 10 epochs. The positioning accuracy of the east and north components is comparable, achieving 1–2 cm across different days, while the positioning accuracy of the up direction is slightly worse, representing 2–6 cm. A similar conclusion can be drawn in terms of convergence time. Moreover, it can also be noticed that the positioning performance is related to the quality of atmospheric corrections, that is, those on the 7th and 8th September are slightly worse than other days. Despite positioning performance variations are noticed, the achieved solutions are still comparable with the state-of-the-art PPP-RTK solutions, demonstrating the applicability of PPP-RTK technology during the selected periods with typhoon Saola and moderate solar activities within Hong Kong, which therefore infer that, similar performance can be expected during similar complex weather events analyzed in this study.

5. Conclusion

The quality of ionospheric and tropospheric corrections significantly affects the PPP-RTK positioning performance. To validate the PPP-RTK applicability during typhoon Saola and moderate geomagnetic and ionospheric disturbances, this study starts with introducing PPP-RTK atmospheric modeling, followed by the correction quality assessment and comparison across different days during typhoon Saola using data from GNSS CORS stations in Hong Kong. Positioning validation is conducted to verify the applicability of PPP-RTK technology under moderate-intensity typhoon event.

The generated ZWD corrections and the built ZWD model are detailed evaluated first. The derived ZWDs for each station match the trend of historical rainfall records, with ZWD differences among different stations below 5 cm in normal days. The ZWD model residuals exhibit good precision across different days, showing medium values of absolute ZWD residuals for different days all around 2 mm. The standard deviations of the ZWD residuals are positively correlated with rainfall caused by typhoon. Moreover, the model accuracy is also affected by the uneven rainfall of different regions in Hong Kong.

The analysis of ionospheric corrections indicates that the ionospheric errors are less related to medium global solar activities inferred by indices such as Kp and Dst. However, ionospheric interpolation errors are found to be correlated with ionospheric disturbances caused by Saola. The interpolated errors increase before and after the

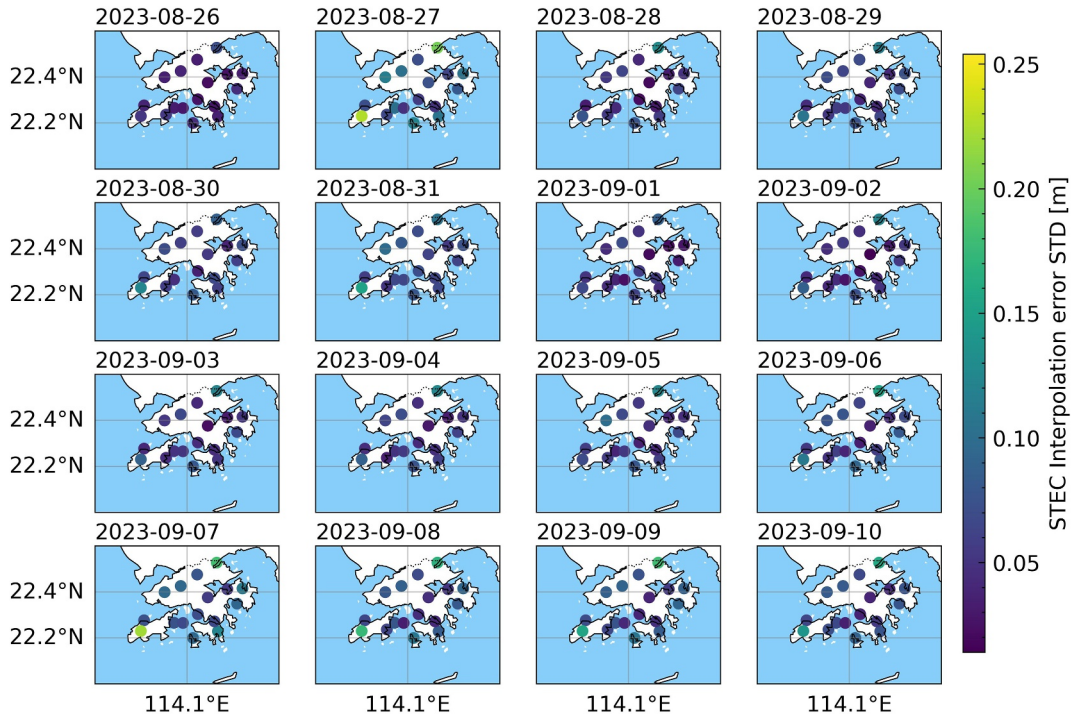

Figure 11. STDs of the slant total electron content interpolation errors for each station on different days.

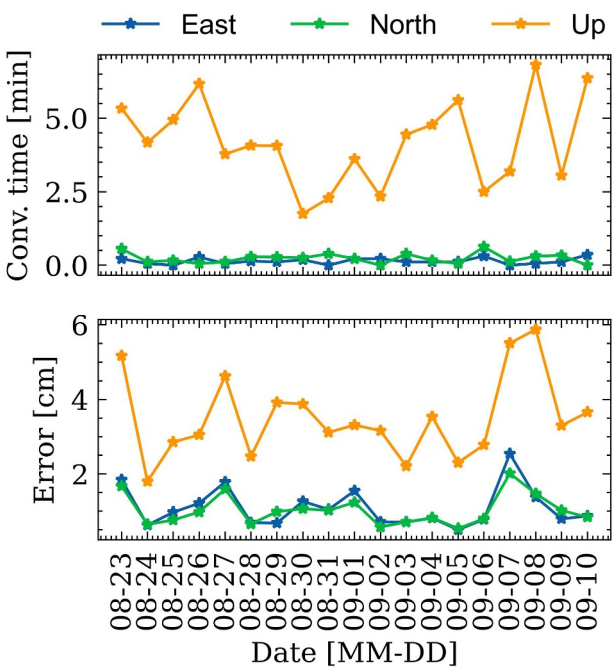

Figure 12. Average positioning performance for different days of all Hong Kong CORS stations with Precise Point Positioning Real-time Kinematic kinematic processing.

landfall, while the precision is the best on the landfall day. The possible reason is that the ionospheric perturbations in the eye of the storm are fewer than those at the edges of the typhoon. Moreover, the interpolation errors for the stations at the edge of Hong Kong are slightly larger than other stations, which is caused by the poor distribution of server stations.

With generated atmospheric corrections, PPP-RTK user positioning validation is carried out. Results show that the positioning accuracy of the east and north components is comparable, achieving 1–2 cm across different days with almost instantaneous convergence, while the positioning accuracy of the up direction is slightly worse, representing positioning accuracy of 2–6 cm which converges for 2–5 min. The solutions achieved are comparable with the state-of-the-art solutions, demonstrating the applicability of PPP-RTK technology during moderate-intensity typhoon events and medium solar activities.

The obtained results in this study provide insight for the GNSS field on the atmospheric quality and applicability of PPP-RTK in typhoon events, which could potentially expand the PPP-RTK applications in meeting various user demands. However, there are still some limitations in this study. Since data from Hong Kong is selected for analysis, the inter-station distance is small, that is, the atmospheric refractions are similar for most time. When expanding the research into a larger scale area, more investigation is needed. Besides, the geomagnetic activity during the assessed period is moderate, and the effect of severe geomagnetic storms (e.g., Kp > 7) on PPP-RTK has not been investigated. Moreover, there is only moderate ionospheric activity during the assessed periods, when severe ionospheric activity occurs, the outlier identification, cycle slip detection, and quality

control methods become more challenging, which could therefore lead to challenge in obtaining reliable PPP-RTK corrections and positioning solutions.

Conflict of Interest

The authors declare no conflicts of interest relevant to this study.

Data Availability Statement

The IMF data are provided from CDAWeb (https://omniweb.gsfc.nasa.gov/form/sc_merge_min1.html). The Dst index are provided by the Goddard Space Flight Center (https://omniweb.gsfc.nasa.gov/). The GNSS data are provided by Hong Kong GNSS network (SatRef) (https://www.geodetic.gov.hk/sc/satref/RINEX_download.htm).

Acknowledgments
This research is supported by the National Natural Science Foundation of China (Grants 42504050, 42374026, 42330717), the Research Funds for the Interdisciplinary Projects, CHU (Grant 300104240914), the Guangdong-Hong Kong Joint Laboratory for Marine Infrastructure (2025B1212150001), and the University Grants Committee of Hong Kong under the General Research Fund (15229622, 152318/22E, 152344/23E). We would like to appreciate Dr. Tong Liu at The Hong Kong Polytechnic University for calculating the ROTI values.

References

Carter, B. A., Pradipta, R., Dao, T., Currie, J. L., Choy, S., Wilkinson, P., et al. (2023). The ionospheric effects of the 2022 Hunga Tonga Volcano eruption and the associated impacts on GPS Precise Point positioning across the Australian region. *Space Weather*, *21*(5), e2023SW003476. https://doi.org/10.1029/2023sw003476

Chen, J., Ren, X., Yang, P., Xu, G., Huang, L., Xiong, S., & Zhang, X. (2023). Global ionospheric modeling based on GNSS, satellite altimetry, radio occultation, and DORIS data considering ionospheric vatiation. *Journal of Geophysical Research: Space Physics*, *128*(10), e2023JA031514. https://doi.org/10.1029/2023ja031514

Chen, P., Liu, H., Ma, Y., & Zheng, N. (2020). Accuracy and consistency of different global ionospheric maps released by IGS ionosphere associate analysis centers. *Advances in Space Research*, *65*(1), 163–174. https://doi.org/10.1016/j.asr.2019.09.042

Cui, B., Wang, J., Li, P., Ge, M., & Schuh, H. (2022). Modeling wide-area tropospheric delay corrections for fast PPP ambiguity resolution. *GPS Solutions*, *26*(2), 56. https://doi.org/10.1007/s10291-022-01243-1

Danilchuk, E., Yasyukevich, Y., Vesnin, A., Klyusilov, A., & Zhang, B. (2025). Impact of the May 2024 extreme geomagnetic storm on the ionosphere and GNSS positioning. *Remote Sensing*, *17*(9), 1492. https://doi.org/10.3390/rs17091492

Demyanov, V., & Yasyukevich, Y. (2021). Space weather: Risk factors for global navigation satellite systems.

Du, X., Zhou, C., Xu, X., Dong, L., Zhang, X., Wang, Z., & Liu, J. (2023). Statistical relationship of ionospheric disturbances caused by typhoon extinction on the sea. *Journal of Geophysical Research: Space Physics*, *128*(11), e2023JA031706. https://doi.org/10.1029/2023ja031706

Freeshah, M., Zhang, X., Şentürk, E., Adil, M., Mousa, B., Tariq, A., et al. (2021). Analysis of atmospheric and ionospheric variations due to impacts of super typhoon mangkhut (1822) in the Northwest Pacific Ocean. *Remote Sensing*, *13*(4), 661. https://doi.org/10.3390/rs13040661

Geng, J., Wen, Q., Zhang, Q., Li, G., & Zhang, K. (2022). GNSS observable-specific phase biases for all-frequency PPP ambiguity resolution. *Journal of Geodesy*, *96*(2), 11. https://doi.org/10.1007/s00190-022-01602-3

He, L., Guo, C., Yue, Q., Zhang, S., Qin, Z., & Zhang, J. (2023). A novel ionospheric disturbance index to evaluate the global effect on BeiDou navigation satellite system signal caused by the moderate geomagnetic storm on May 12, 2021. *Sensors*, *23*(3), 1183. https://doi.org/10.3390/s23031183

Hu, J., Cui, B., Li, P., Bisnath, S., & Zheng, K. (2023). Exploring the role of PPP-RTK network configuration: A balance of server budget and user performance. *GPS Solutions*, *27*(4), 184. https://doi.org/10.1007/s10291-023-01518-1

Hu, J., Shi, Y., Li, P., Chen, W., Tang, L., Zhou, F., et al. (2025). Effect of constraining a limited number of slant ionospheric corrections in PPP and an improved partial tight-constraining Algorithm. *IEEE Transactions on Aerospace and Electronic Systems*, 1–13. https://doi.org/10.1109/TAES.2025.3649142

Hu, J., Zhang, X., Li, P., Ma, F., & Pan, L. (2020). Multi-GNSS fractional cycle bias products generation for GNSS ambiguity-fixed PPP at Wuhan University. *GPS Solutions*, *24*, 1–13. https://doi.org/10.1007/s10291-019-0929-9

Huang, G., Du, S., & Wang, D. (2023). GNSS techniques for real-time monitoring of landslides: A review. *Satell Navig*, *4*(1), 5. https://doi.org/10.1186/s43020-023-00095-5

Huang, J., Li, X., Li, X., Han, J., Liang, D., & Zhang, W. (2025). Quality monitoring of grid-based atmospheric corrections in GNSS PPP-RTK service using leave-one-out cross-validation. *Satellite Navigation*, *6*(1), 25. https://doi.org/10.1186/s43020-025-00178-5

Klobuchar, J. (1987). Ionospheric time-delay algorithm for single-frequency GPS users. *IEEE Transactions on Aerospace and Electronic Systems* (3), 325–331. https://doi.org/10.1109/taes.1987.310829

Kouba, J. (2009). A guide to using International GNSS Service (IGS) products. https://igscb.jpl.nasa.gov/igscb/resource/pubs/UsingIGSProductsVer21.pdf

Kouba, J., & Héroux, P. (2001). Precise point positioning using IGS orbit and clock products. *GPS Solutions*, *5*(2), 12–28. https://doi.org/10.1007/pl00012883

Li, K., Zhang, D., Zeng, Y., Tian, Y., Dai, G., Liu, Z., et al. (2024). Revisiting the ionospheric disturbances over low latitude region of China during super typhoon Hato. *Space Weather*, *22*(5), e2023SW003694. https://doi.org/10.1029/2023sw003694

Li, P., Cui, B., Hu, J., Liu, X., Zhang, X., Ge, M., & Schuh, H. (2022). PPP-RTK considering the ionosphere uncertainty with cross-validation. *Satellite Navigation*, *3*(1), 10–13. https://doi.org/10.1186/s43020-022-00071-5

Li, W., Li, Z., Wang, N., Liu, A., Zhou, K., Yuan, H., & Krankowski, A. (2022). A satellite-based method for modeling ionospheric slant TEC from GNSS observations: Algorithm and validation. *GPS Solutions*, *26*(1), 14. https://doi.org/10.1007/s10291-021-01191-2

Li, W., Liu, T., Zuo, P., Zou, Z., Ruan, M., & Wei, J. (2024b). *Low-latitude ionospheric responses and positioning performance of ground gnss associated with the geomagnetic storm on march 13-14, 2022*. Frontiers in Astronomy and Space Sciences.

Li, W., Song, S., Bai, T., Cheng, N., Zhou, W., & Yu, C. (2025). Mitigating the impacts of ionospheric irregularities on GPS precise positioning by refined cycle slip threshold. *GPS Solutions*, *29*(3), 128. https://doi.org/10.1007/s10291-025-01888-8

Li, W., Yue, J., Yang, Y., Li, Z., Guo, J., Pan, Y., & Zhang, K. (2017). Analysis of ionospheric disturbances associated with powerful cyclones in East Asia and North America. *Journal of Atmospheric and Solar-Terrestrial Physics*, *161*, 43–54. https://doi.org/10.1016/j.jastp.2017.06.012

Li, X., Wang, B., Li, X., Huang, J., Lyu, H., & Han, X. (2022). Principle and performance of multi-frequency and multi-GNSS PPP-RTK. *Satellite Navigation*, *3*(1), 7. https://doi.org/10.1186/s43020-022-00068-0

Luo, X., Du, J., Galera Monico, J. F., Xiong, C., Liu, J., & Liang, X. (2022). ROTI-based stochastic model to improve GNSS precise point positioning under severe geomagnetic storm activity. *Space Weather*, *20*(7), e2022SW003114. https://doi.org/10.1029/2022sw003114

Luo, X., Du, J., Lou, Y., Gu, S., Yue, X., Liu, J., & Chen, B. (2022). A method to mitigate the effects of strong geomagnetic storm on GNSS precise point positioning. *Space Weather*, *20*(1), e2021SW002908. https://doi.org/10.1029/2021sw002908

Luo, X., Gu, S., Lou, Y., et al. (2018). Assessing the performance of gps precise point positioning under different geomagnetic storm conditions during solar cycle 24. *Sensors*.

Ma, H., Zhao, Q., Verhagen, S., Psychas, D., & Liu, X. (2020). Assessing the performance of multi-GNSS PPP-RTK in the local area. *Remote Sensing*, *12*(20), 3343. https://doi.org/10.3390/rs12203343

Moreno, B., Radicella, S., de Lacy, M. C., Herraiz, M., & Rodriguez-Caderot, G. (2011). On the effects of the ionospheric disturbances on precise point positioning at equatorial latitudes. *GPS Solutions*, *15*(4), 381–390. https://doi.org/10.1007/s10291-010-0197-1

Nie, W., Wang, F., Qiao, Z., Xu, T., Wang, Y., Ye, M., & Liu, T. (2024). Ionospheric irregularities coinciding with the 2023 Typhoon Saola: A multi-instrument study. *Journal of Geophysical Research: Space Physics*, *129*(12), e2024JA033043. https://doi.org/10.1029/2024ja033043

Odijk, D., Zhang, B., Khodabandeh, A., Odolinski, R., & Teunissen, P. (2016). On the estimability of parameters in undifferenced, uncombined GNSS network and PPP-RTK user models by means of S -system theory. *Journal of Geodesy*, *90*(1), 15–44. https://doi.org/10.1007/s00190-015-0854-9

Paziewski, J., Høeg, P., Sieradzki, R., Jin, Y., Jarmolowski, W., Hoque, M. M., et al. (2022). The implications of ionospheric disturbances for precise GNSS positioning in Greenland. *Journal of Space Weather and Space Climate*, *12*, 33. https://doi.org/10.1051/swsc/2022029

Qu, X., Ding, X., Yu, W., Li, X., & Xu, Y. (2025). High-rate bridge displacement monitoring with low-rate virtual reference station data. *GPS Solutions*, *29*(1), 8. https://doi.org/10.1007/s10291-024-01766-9

Rodríguez Bilbao, I., Radicella, S. M., Rodríguez-Caderot, G., & Herraiz, M. (2015). Precise point positioning performance in the presence of the 28 October 2003 sudden increase in total electron content. *Space Weather*, *13*(10), 698–708. https://doi.org/10.1002/2015sw001201

Teunissen, P., Odijk, D., & Zhang, B. (2010). PPP-RTK: Results of CORS network-based PPP with integer ambiguity resolution. *Journal of Aeronautics, Astronautics and Aviation. Series A*, *42*(4), 223–230.

Wu, J., Wu, S., Hajj, G., Bertiger, W., & Lichten, S. (1993). Effects of antenna orientation on GPS carrier phase. *Manuscripta Geodaetica*, *18*(2), 91–98. https://doi.org/10.1007/bf03655303

Wübbena, G., Schmitz, M., & Bagge, A. (2005). PPP-RTK: Precise point positioning using state-space representation in RTK networks. In *Proceedings of ION GNSS-05, Institute of Navigation, Inc., Fairfax, USA* (pp. 2584–2594).

Xu, J., Ke, F., Zhao, X., & Qi, X. (2020). Characteristics of the ionospheric disturbances caused by typhoon using GPS and ionospheric sounding. In J. Shen, Y. C. Chang, Y. S. Su, & H. Ogata (Eds.), *Cognitive cities. IC3 2019. Communications in computer and information science* (Vol. 1227, pp. 509–517). Springer. https://doi.org/10.1007/978-981-15-6113-9_57

Xue, D., Zhang, Q., Feng, X., & Wang, C. (2025). Space weather and low-altitude drone economy. *Space Weather*, *24*(1), e2025SW004803. https://doi.org/10.1029/2025sw004803

Yu, S., Liu, Z., & Lee, T. (2022). Ionospheric disturbances observed from a single GPS station in Hong Kong during the passage of Super Typhoon Hato in 2017. *Space Weather*, *20*(1), e2021SW002850. https://doi.org/10.1029/2021sw002850

Zhang, X., Ren, X., Chen, J., Zuo, X., Mei, D., & Liu, W. (2022). Investigating GNSS PPP-RTK with external ionospheric constraints. *Satellite Navigation*, *3*(1), 6. https://doi.org/10.1186/s43020-022-00067-1

Zhang, X., Yang, Y., Yang, H., Ren, X., Lin, X., Le, X., & Li, X. (2025). Performance of PPP and PPP-RTK with new-generation GNSS constellations and signals. *Satell Navig*, *6*(1), 17. https://doi.org/10.1186/s43020-025-00169-6